ANALYSIS OF WIND TUNNEL CORRECTIONS FOR HALF-MODEL TESTS OF A TRANSPORT AIRCRAFT USING A DOUBLET PANEL METHOD*

M. Mokry and J. R. Digney
National Aeronautical Establishment
National Research Council of Canada
Ottawa, Ontario

R. J. D. Poole
The de Havilland Aircraft Company of Canada
A Division of Boeing Canada Ltd.
Downsview, Ontario

Abstract

A correction method is described for half-model tests using wall pressures measured by longitudinal static pressure tubes, and measured model forces. The Dirichlet problem for the Mach number correction is solved by a doublet panel method and the flow angle corrections are obtained from the irrotational flow conditions.

The method is applied to a transport aircraft half-model tested in the NAE perforated wall wind tunnel. The Mach number and angle of attack corrections are presented as contour plots, allowing analysis of the effects of wall induced gradients. In the range of normal operating lift coefficients, the corrected drag polar is shown to correlate well with data from full-model wind tunnel tests and from the flight test aircraft.

Symbols

A_{kj}	panel influence matrix
C_D	model drag coefficient
C_L	model lift coefficient
C_p	pressure coefficient
c	mean aerodynamic chord (=7.25 in)
f	doublet density
F	half-model fuselage cross-sectional area
M	stream Mach number
$\overline{n}$	outward (unit) normal vector
N	number of panels
q	dynamic pressure
$\overline{r}$	position vector
Re	Reynolds number based on c
S	test section boundary
S_R	half-model wing reference area (= 293 in^2)
U	stream velocity (= 1)
u, v, w	components of wall interference velocity
X, Y, Z	Cartesian coordinates in the physical plane
x, y, z	Cartesian coordinates in the transformed plane
α	angle of attack
β	$\sqrt{1-M^2}$
γ	ratio of specific heats
δ	increment due to reference pressure error
Δ	wall interference correction
ξ, η, ς	local (panel) coordinates
ϕ	disturbance velocity potential
ψ	sideslip angle

Subscripts

F	free air
j, k	collocation points
N	model nose
o	observation (field) point
R	reference plane
T	model tail
W	wall interference
1, 2	panel corners

Introduction

The major advantages of half-model testing over full-model testing are the higher model Reynolds number and the larger instrumentation space that can be realized with a larger-scale model in a test section of a given size. The well known weaknesses of the technique are the influence of the tunnel wall boundary layer on the flow over the half-fuselage and a relatively large wall interference from the surrounding walls. The present paper, prompted by the general interest in high Reynolds number testing, is devoted to the topic of wall interference.

The wind tunnel data of the transport aircraft half-model were produced in the 5-ft × 5-ft transonic test section of the National Aeronautical Establishment (NAE) Trisonic Blowdown Wind Tunnel. The model configuration was selected to permit correlation with data from concurrent tests of a large 3-D model and aircraft flight tests. The walls of the test section are perforated by normal holes of 0.5 inch diameter, providing an open area ratio of 20.5%. A solid (reflection) plate, with elliptic leading edge, was installed

* This R&D was jointly supported by the de Havilland Aircraft Company of Canada, a Division of Boeing Canada Ltd., and by the PILP Office of the National Research Council of Canada.

on the North wall of the test section. The other three perforated walls were left unobstructed, allowing the tunnel flow to interact with the surrounding plenum. A photograph of one of the model versions installed in the test section is shown in Fig.1. The NAE 5-component sidewall balance provided the primary model support and pitching mechanism. The half-model was equipped with a 0.75 inch filler plate, to compensate for the displacement effect of the wall boundary layer.

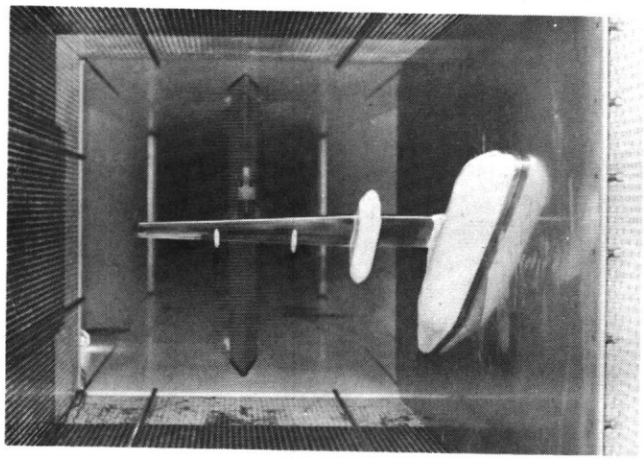

Figure 1. Model Installation in NAE 5-ft Wind Tunnel

Since the 42 inch span of the half-model accounted for nearly 75% of the test section width, it was not surprising that the analysis of the first phase (1982) of test data revealed the presence of substantial wall interference. Correlation of the half-model (reflection plane) data with data from tests of a full model spanning 72% of the NAE 30-ft solid wall wind tunnel, and with flight test data showed drag coefficients and induced drag factors to be significantly and consistently too large.

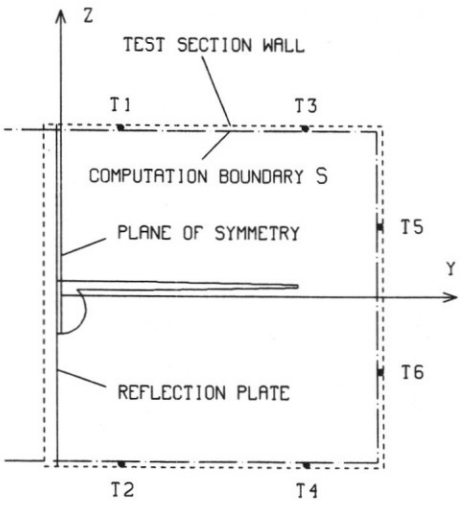

Figure 2. Coordinate System

Therefore, in the second test phase (1983) of the half-model, four available longitudinal static pressure tubes (rails) were installed on the floor and ceiling of the 5-ft × 5-ft test section to obtain boundary data suitable for wall interference assessment. For the third phase (1985), two additional pressure tubes were manufactured and mounted on the sidewall to improve the boundary data input near the wing tip. This most recent configuration is shown schematically in Fig.2. The tubes were positioned both on the basis of theoretical predictions and mechanical constraints dictated by the location of the wall perforations and structural components of the wind tunnel. The transverse coordinates of the pressure orifices ($Y = 0$ is the model plane of symmetry) are given in Table 1.

Tube	Y(in)	Z(in)
T1	10.62	29.00
T2	10.62	-29.00
T3	43.38	29.00
T4	43.38	-29.00
T5	56.00	12.30
T6	56.00	-13.20

Table 1. Pressure Orifice Locations

The cross-section of the 1-in diameter tube is shown in Fig.3. Each tube provides a single row of 40 static pressure taps over a distance of 120 inches, distributed more densely in the region of the model. The pressures were scanned with two Scanivalve assemblies and measured differentially against the plenum pressure, which, together with the measured stagnation pressure at the settling chamber, were used to define the tunnel stream Mach number, M.

The wall correction technique, which is conceptually similar to the methods of Refs.(1) and (2), was developed at NAE and is described in greater detail in Ref.(3).

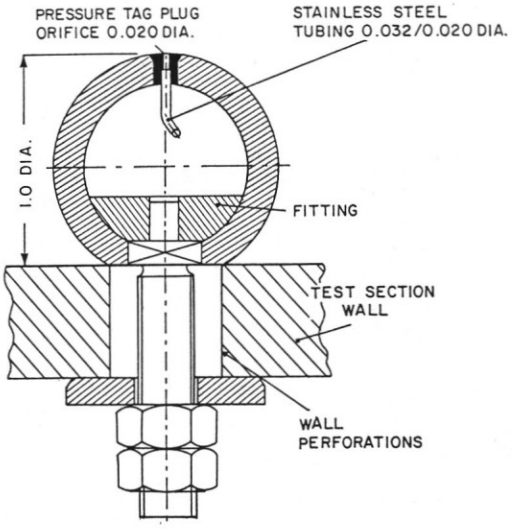

Figure 3. Cross-Section of NAE Static Pressure Tube

Correction Method

In accordance with the wall interference concept[1], we assume that in a region adjacent to the test section walls the flow can be described by the linearized potential equation

$$\beta^2 \frac{\partial^2 \phi}{\partial X^2} + \frac{\partial^2 \phi}{\partial Y^2} + \frac{\partial^2 \phi}{\partial Z^2} = 0. \qquad (1)$$

The disturbance velocity potential ϕ, which satisfies the pressure boundary conditions at the walls, is decomposed into two parts:

$$\phi = \phi_F + \phi_W, \qquad (2)$$

where ϕ_F is the disturbance potential of the model in free air and ϕ_W is the disturbance potential representing the effect of tunnel walls. It is further assumed that ϕ_W is non-singular, satisfying Eq.(1) in the entire test section interior, including the volume occupied by the model. Accordingly, the interference velocity components

$$u = \frac{\partial \phi_W}{\partial X}, \quad v = \frac{\partial \phi_W}{\partial Y}, \quad w = \frac{\partial \phi_W}{\partial Z} \qquad (3)$$

can be interpreted as velocity disturbances to the uniform stream. Because of differentiability of harmonic functions, the interference velocity components inside the test section again satisfy

$$\beta^2 \frac{\partial^2 u}{\partial X^2} + \frac{\partial^2 u}{\partial Y^2} + \frac{\partial^2 u}{\partial Z^2} = 0, \qquad (4)$$

and so on.

The boundary values of the streamwise component of wall interference velocity, u, are obtained from measured boundary pressures and the farfield of the free air potential[1]. From Eqs.(2) and (3) accordingly:

$$u = \frac{\partial \phi_W}{\partial X} = \frac{\partial \phi}{\partial X} - \frac{\partial \phi_F}{\partial X} = -\frac{1}{2} C_p - \frac{\partial \phi_F}{\partial X}, \qquad (5)$$

where C_p is the (linearized) pressure coefficient.

Typical pressure distributions obtained for the de Havilland half-model at $M = 0.450$ and $C_L = 0.551$ (based on $S_R = 293$ in^2) are presented in Fig.4.

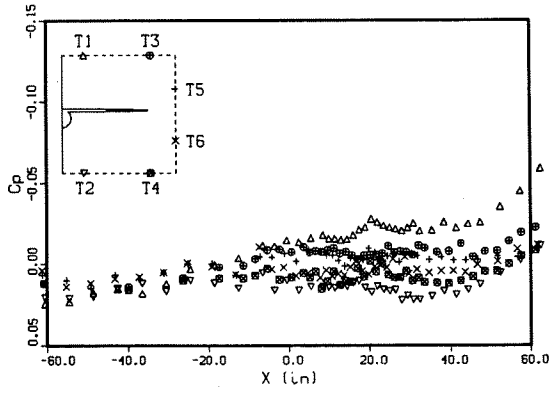

Figure 4. Tube Pressure Distributions
$M = 0.450$, $\alpha = 1.247^0$, $C_L = 0.551$

The potential ϕ_F on the boundary is approximated by a small number of internal singularities, representing the shape of the model and the spanwise distribution of measured aerodynamic forces[2],[3].

The boundary values of u, evaluated along the static pressure tubes, are then smoothed and expanded over the test section bounding surface accounting for symmetry, $\partial u/\partial Y = 0$ at $Y = 0$, and using suitable interpolations[3].

The interior Dirichlet problem specified by Eqs.(4) and (5) can be solved by a number of numerical techniques. To facilitate the doublet panel approach, which appears to be particularly attractive, we use the compressibility transformation

$$x = X, \quad y = \beta Y, \quad z = \beta Z \qquad (6)$$

reducing Eq.(4) to Laplace's equation, $\nabla^2 u = 0$. Introducing the position vectors

$$\bar{r}_o = (x_o, y_o, z_o) \qquad \text{and} \qquad \bar{r} = (x, y, z)$$

of the observation point and the running point respectively, the streamwise component of the wall interference velocity can be expressed in terms of a double layer distribution

$$u(\bar{r}_o) = \iint_S f(\bar{r}) \frac{\partial}{\partial n} \left(\frac{1}{4\pi |\bar{r}_o - \bar{r}|} \right) dS, \qquad (7)$$

the scalar function f is the doublet density and $\partial/\partial n$ is the outward normal derivative. The bounding surface S is a box enclosing the model, formed by the horizontal and vertical planes passing through the pressure orifice lines, Fig.2, their symmetry plane images, and the upstream and downstream faces. The symmetry plane $y = 0$ is not a part of the bounding surface.

In the limit $\bar{r}_o \to \bar{r}_k \in S$, as the observation point $\bar{r}_o$ approaches a smooth surface point $\bar{r}_k$, Eq.(7) becomes the Fredholm integral equation of the second kind for the doublet density[4]:

$$u(\bar{r}_k) = -\frac{1}{2} f(\bar{r}_k) + \iint_S f(\bar{r}) \frac{\partial}{\partial n} \left(\frac{1}{4\pi |\bar{r}_k - \bar{r}|} \right) dS. \qquad (8)$$

The integral equation is solved numerically by the first-order doublet panel method. The division of the real test section surface into $N/2 = 215$ rectangular panels, used in the present paper, is shown in Fig.5.

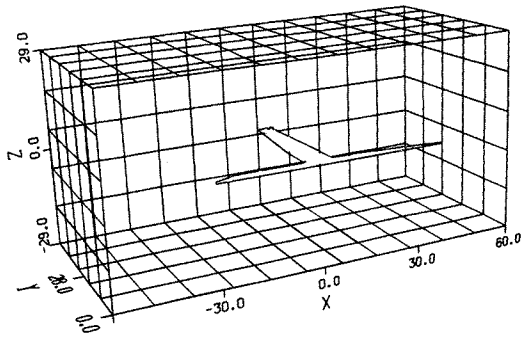

Figure 5. Test Section Panelling

The surface distribution of the boundary values u, constructed from the tube pressure data of Fig.4, is displayed on the unfolded half-surface in Fig.6. In this graphical display, the number of shading lines of each panel was made equal to the value $1000 \times |u|$ at the centroid, with the sign indicated by the orientation of the lines.

Turning back to to Eq.(8), we denote the surface panels by S_j, $(j = 1, \ldots, N)$, and use piecewise constant doublet densities,

$$f(\bar{r}) = f_j, \qquad \bar{r} \in S_j.$$

Since

$$\frac{\partial}{\partial n}\frac{1}{|\bar{r}_k - \bar{r}|} = \frac{\bar{n}\cdot(\bar{r}_k - \bar{r})}{|\bar{r}_k - \bar{r}|^3} = 0 \qquad \text{if} \qquad \bar{r}, \bar{r}_k \in S_j,$$

Eq.(8) reduces to

$$u(\bar{r}_k) = -\frac{1}{2}f_k + \sum_{\substack{j=1 \\ j\neq k}}^{N} f_j \iint_{S_j} \frac{\partial}{\partial n}\left(\frac{1}{4\pi|\bar{r}_k - \bar{r}|}\right) dS. \quad (9)$$

Selecting $\bar{r}_k$ to be the panel centroids and denoting $u(\bar{r}_k) = u_k$, we obtain the system of linear algebraic equations

$$\sum_{j=1}^{N} A_{kj} f_j = u_k, \qquad k = 1, \ldots, N \quad (10)$$

for the N unknown values of doublet densities f_j. The matrix element

$$A_{kj} = \begin{cases} -\frac{1}{2}, & \text{if } j = k; \\ \displaystyle\iint_{S_j} \frac{\partial}{\partial n}\left(\frac{1}{4\pi|\bar{r}_k - \bar{r}|}\right) dS, & \text{if } j \neq k \end{cases} \quad (11)$$

is evaluated for rectangular panels using the integral[3]:

$$\int_{\eta_1}^{\eta_2}\int_{\xi_1}^{\xi_2} \frac{\partial}{\partial \varsigma}\frac{1}{4\pi\sqrt{(\xi_o-\xi)^2+(\eta_o-\eta)^2+(\varsigma_o-\varsigma)^2}}\Big|_{\varsigma=0} d\xi d\eta$$

$$= \frac{1}{4\pi}\Big\{ \arctan\Big[\frac{\xi_o-\xi_1}{\varsigma_o}\frac{\eta_o-\eta_1}{\sqrt{(\xi_o-\xi_1)^2+(\eta_o-\eta_1)^2+\varsigma_o^2}}\Big] - \arctan\Big[\frac{\xi_o-\xi_1}{\varsigma_o}\frac{\eta_o-\eta_2}{\sqrt{(\xi_o-\xi_1)^2+(\eta_o-\eta_2)^2+\varsigma_o^2}}\Big] - \arctan\Big[\frac{\xi_o-\xi_2}{\varsigma_o}\frac{\eta_o-\eta_1}{\sqrt{(\xi_o-\xi_2)^2+(\eta_o-\eta_1)^2+\varsigma_o^2}}\Big] + \arctan\Big[\frac{\xi_o-\xi_2}{\varsigma_o}\frac{\eta_o-\eta_2}{\sqrt{(\xi_o-\xi_2)^2+(\eta_o-\eta_2)^2+\varsigma_o^2}}\Big]\Big\}, \quad (12)$$

which is the contribution of the rectangular panel $\xi_1 < \xi < \xi_2$, $\eta_1 < \eta < \eta_2$, $\varsigma = 0$ at $\xi_o, \eta_o, \varsigma_o$. In the limit $\varsigma_o \to 0-$ the integral gives $-\frac{1}{2}$, in agreement with the case $j = k$ in Eq.(11).

Because of symmetry, there is a duplication in the matrix elements which allows the system of equations to be reduced by half (back to $N/2$).

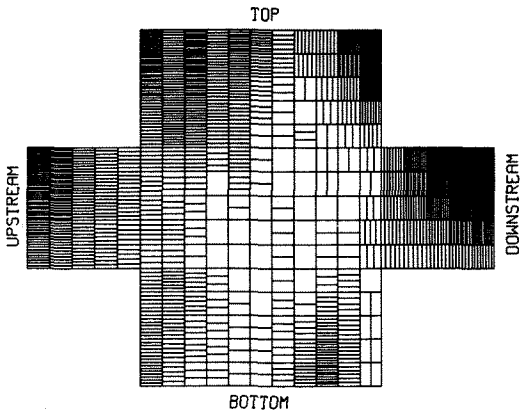

Figure 6. Boundary Values of u
$M = 0.450$, $\alpha = 1.247^0$, $C_L = 0.551$

Once the doublet densities are known, the value of the streamwise component of the wall interference velocity can be calculated at any point $\bar{r}_o$ inside the test section using the discrete form of integral (7):

$$u(\bar{r}_o) = \sum_{j=1}^{N} f_j \iint_{S_j} \frac{\partial}{\partial n}\left(\frac{1}{4\pi|\bar{r}_o - \bar{r}|}\right) dS. \quad (13)$$

The integrals over S_j, representing the individual contributions of the panels, are again evaluated using Eq.(12).

The transverse components of interference velocity are calculated by integrating the irrotational flow conditions[2]:

$$v(X,Y,Z) - v(X_R,Y,Z) = \int_{X_R}^{X} \frac{\partial u}{\partial Y}(\xi,Y,Z)d\xi,$$
$$w(X,Y,Z) - w(X_R,Y,Z) = \int_{X_R}^{X} \frac{\partial u}{\partial Z}(\xi,Y,Z)d\xi, \quad (14)$$

where X_R is the X-coordinate of the reference plane. As indicated, v and w can be determined from Eqs.(14) at any point X, Y, Z inside the test section, provided that their reference-plane values are known. An illustrative example of an experimental flow angle distribution in a crossflow plane has been given[5], but in 'production' testing it is often necessary to assume parallel flow at the reference plane:

$$\frac{\partial \phi}{\partial Y}(X_R,Y,Z) = 0, \quad \frac{\partial \phi}{\partial Z}(X_R,Y,Z) = 0. \quad (15)$$

Inserting Eqs.(2) and (15) in (3), we obtain the reference-plane values

$$v(X_R,Y,Z) = -\frac{\partial \phi_F}{\partial Y}(X_R,Y,Z),$$
$$w(X_R,Y,Z) = -\frac{\partial \phi_F}{\partial Z}(X_R,Y,Z). \quad (16)$$

Differentiating Eqs.(15) in the Y and Z directions respectively and substituting them in Eq.(1), we verify that Eqs.(16) are permissible upstream boundary conditions if

$$\frac{\partial^2 \phi}{\partial X^2}(X_R, Y, Z) = -\frac{1}{2}\frac{\partial C_p}{\partial X}(X_R, Y, Z) = 0, \qquad (17)$$

that is, if the measured streamwise pressure curves display zero slopes at the reference plane. Experimental wall pressure coefficients in Fig.4 meet this requirement satisfactorily by approaching a nearly constant level at the upstream end.

One of the attractive features of the doublet panel method is that the interference velocity components v and w are again obtained by summing the individual contributions of the panels. Formally, this is accomplished by substituting Eq.(13) in Eqs.(14) and transposing $\sum f_j \iint_{S_j}$ in front. Unlike the integral (12), expressing the unit density panel contribution to u, we were not able to obtain similar contributions to v and w in closed form, and had to use a rectangular rule.

From the computed distribution of u the Mach number correction is obtained as[6]

$$\Delta M = (1 + \frac{\gamma - 1}{2} M^2) M u, \qquad (18)$$

where M is the reference Mach number and $\gamma (= 1.4)$ is the ratio of specific heats. The sideslip angle and angle of attack corrections (in radians) are directly the values of v and w respectively:

$$\Delta\psi = v, \quad \Delta\alpha = w. \qquad (19)$$

These corrections are evaluated at some representative model station (centre of loading) or as averages over the model and applied to tunnel stream parameters to obtain equivalent free air conditions for the particular test. Using $\Delta\alpha$, the measured aerodynamic force is resolved into corrected directions parallel and normal to the flow, to obtain the true values of drag and lift. The force and moment coefficient corrections due to the dynamic pressure adjustment, Δq, are obtained by multiplying the coefficients by the factor[6]

$$-\Delta q/q = -(2 - M^2)u. \qquad (20)$$

The spatial variations of u, v, and w are used to estimate the residual effects due to wall induced flow nonuniformities. The buoyancy drag coefficient correction, required to compensate for the axial distribution of the pressure coefficient correction, $\Delta C_p = 2u$, is obtained as follows:

$$\Delta C_D = \frac{1}{S_R}\int_{X_N}^{X_T} 2uF'dX, \qquad (21)$$

where S_R is the half-model reference area, $F = F(X)$ is the axial distribution of half-fuselage frontal area, and X_N and X_T are the nose and tail coordinates.

An important feature of the method is its autocorrective property[1],[9], allowing the use of plenum pressure, or other pressure close enough to the upstream static pressure, as reference. To illustrate this, we denote by δU the initial error of the unit reference velocity U. The corresponding error of the measured wall pressure coefficient C_p, reflecting the changes of stream static and dynamic pressures, is[6]

$$\delta C_p = \left[2 - (2 - M^2)C_p\right]\delta U$$
$$\simeq 2\delta U \quad \text{if} \quad (1 - \frac{M^2}{2})C_p \ll 1.$$

From Eq.(5) we see that the incremental correction

$$\delta u = -\frac{1}{2}\delta C_p = -\delta U$$

compensates for the reference velocity error. However, with respect to the buoyancy drag correction, Eq.(21), it is imperative to satisfy

$$\int_{X_N}^{X_T} F'dX = F(X_T) - F(X_N) = 0,$$

to ensure that a constant u does not contribute to ΔC_D.

Results and Discussion

To avoid irregularities of the computed correction near panel boundaries (singular lines), the computation (grid) points were selected such that their orthogonal projections on the walls coincided with panel centroids. Data on a refined mesh were obtained using splines. The contour lines were generated and plotted by the DISSPLA Version 9.0 package.

Examples of corrections ΔM and $\Delta\alpha$ evaluated in the horizontal plane $Z = 0$ and the vertical plane $X = 0$ are shown in Figs.7 and 8. The total CPU time, including the generation of the matrix, solution of linear equations, and producing the above contour plots was about 10 secs on an IBM 3090. No $\Delta\psi$ corrections were produced and analyzed at this stage, although the procedure would have been very similar to that for $\Delta\alpha$.

The Mach number correction in the upper portion of Fig.7 is observed to be small ($\Delta M \simeq -0.001$) and fairly uniform over the wing planform. The longitudinal variation of ΔM along the fuselage indicates the presence of a buoyancy force on the model. Since the flow in the wind tunnel was accelerated over the model (a negative ΔM correction is required at the nose and a positive correction at the tail), the measured drag force coefficient required a negative correction ($\Delta C_D \simeq -0.0011$).

The lower portion of Fig.7 shows the distribution of the angle of attack correction. The value $\Delta\alpha \simeq -0.35^0$ near the wing centre is moderate by NAE two-dimensional testing experience[7] but the spanwise flow angle variation, being in excess of 0.1^0, is somewhat larger than desired[8].

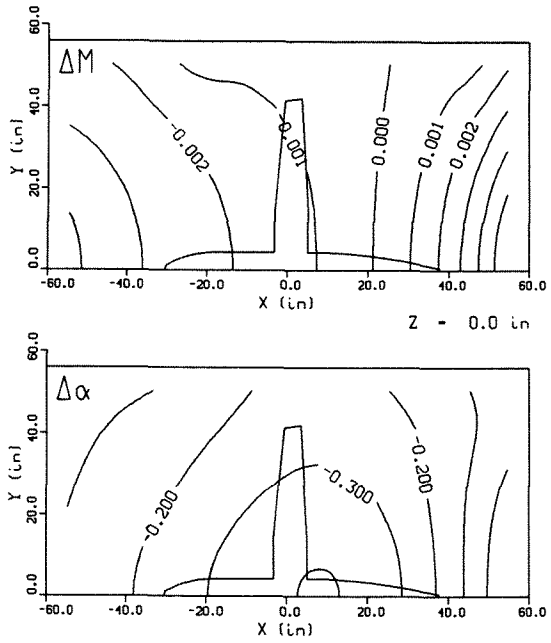

Figure 7. ΔM **and** $\Delta\alpha$ **in the Horizontal Plane**
$M = 0.450$, $\alpha = 1.247^0$, $C_L = 0.551$

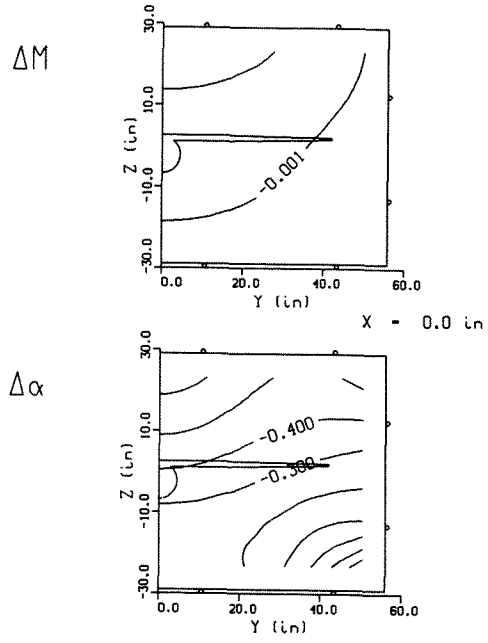

Figure 8. ΔM **and** $\Delta\alpha$ **in the Vertical Plane**
$M = 0.450$, $\alpha = 1.247^0$, $C_L = 0.551$

The downstream gradients of ΔM and $\Delta\alpha$, resulting from the trend of measured pressures towards negative values at the test section exit, see Fig.4, are believed to influence the model data only indirectly, via trailing shear layers.

Figure 8 illustrates the variations of corrections above and below the half-model. Concerning the plot of $\Delta\alpha$, it is worth observing that the peak value occurs at the test section boundary and not on the plane of symmetry (as Fig.7 might suggest), in accordance with the maximum-minimum principle for the Laplace equation.

The summary plot of the corrections to Mach number, angle of attack, and the correction for buoyancy drag are shown for the Phase 3 tests (six pressure tubes) in Fig.9. Here the values of ΔM and $\Delta\alpha$ represent correction values at the centre of theoretical (elliptical) wing loading, whereas ΔC_D is obtained from the distribution of u along the fuselage axis.

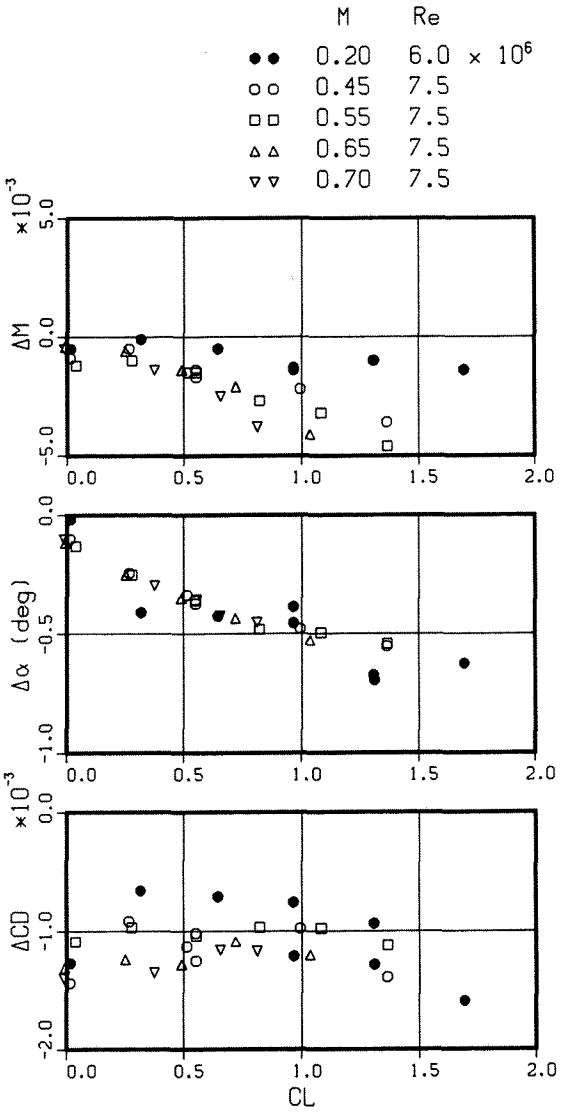

Figure 9. Summary of Corrections

The Mach number correction is seen to be a function of M and C_L. The strong dependence of ΔM on C_L, observed earlier in two-dimensional testing[7], can be explained by different resistance of normally perforated walls to inflow and outflow.

The angle of attack correction, with the exception of the high stagnation pressure case $M = 0.2$, appears to be independent of M and fairly linear up to about $C_L = 0.8$. It is worth commenting that the previously evaluated Phase 2 tests, using only pressure tubes on top and bottom walls, showed similar results: the interpolation of sidewall boundary values from their corner values did not seem to influence the global corrections significantly.

The buoyancy drag correction is more or less constant, independent of both C_L and M. It should be noted, however, that the correction process did not take into account the pitching of the fuselage axis.

Figure 10 presents a comparison of drag polars for the aircraft feathered descent and wind tunnel tests. The flight data and the 30-ft wind tunnel measurements of a complete model are in good agreement for $0.5 < C_L^2 < 1.5$. Outside this range the 30-ft tunnel data deviated significantly from a straight-line relationship. The data from the 5-ft×5-ft wind tunnel gave a far more linear relationship, but the uncorrected drag level was much too high. With wall interference corrections applied, a satisfactory correlation of half-model data with the flight data has been achieved.

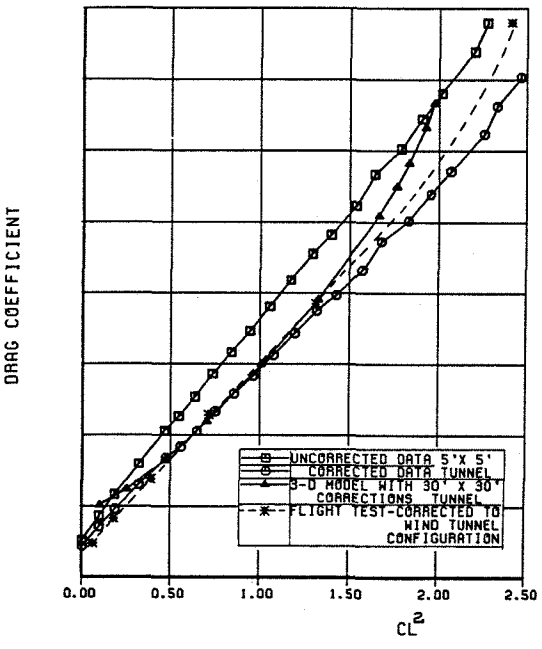

Figure 10. Drag Data Comparison, $M = 0.2$

Conclusions

A linear method has been described for the evaluation of wall interference corrections for half-model configurations at subcritical conditions at perforated test section walls. Input data required for the method are boundary pressures measured by a few longitudinal static pressure tubes, global geometrical parameters of the model and measured forces. The corrections are obtained with no reference to the crossflow properties of the walls.

Sources of inaccuracy of the method are:

(a) simplified treatment of wall interference as corrections to free stream,
(b) farfield representation of the model by internal singularities,
(c) interpolation of sparse boundary data over the test section bounding surfaces,
(d) approximate upstream boundary conditions, and
(e) numerical errors of the first-order panel method.

In spite of these shortcomings, the half-model drag data corrected by the present method were shown to correlate reasonably well with those from flight tests and wind tunnel measurements of a complete model. The paper thus demonstrates that a routine post-test assessment of wall interference effects on half-model test data is feasible using a simple doublet panel method in conjunction with boundary pressure measurements.

References

1. Capelier, C., Chevallier, J.P., and Bouniol, F., "Nouvelle méthode de correction des effets de parois en courant plan," La recherche aérospatiale, Jan.-Feb. 1978, pp.1-11.
2. Rizk, M.H. and Smithmeyer, M.G., "Wind-Tunnel Interference Corrections for Three-Dimensional Flows," Journal of Aircraft, Vol.19, June 1982, pp.465-472.
3. Mokry, M., "Subsonic Wall Interference Corrections for Half-Model Tests Using Sparse Wall Pressure Data," Aeronautical Rept. LR-616, National Research Council Canada, Nov.1985.
4. Stakgold, I., *Green's Functions and Boundary Value Problems*, John Wiley, 1979, pp.513-514.
5. Starr, R.F., "Experimental Observations of Wall Interference at Transonic Speeds," AIAA Paper 78-164, Jan.1978.
6. Garner, H.C., Rogers, E.W.E., Acum, W.E.A., and Maskell, E.C., "Subsonic Wind Tunnel Wall Corrections," AGARDograph 109, Oct.1966, pp.317-321.
7. Mokry, M. and Ohman, L.H., "Application of the Fast Fourier Transform to Two-Dimensional Wind Tunnel Wall Interference," Journal of Aircraft, Vol.17, June 1980, pp.402-408.
8. Steinle, F. and Stanewsky, E., "Wind Tunnel Flow Quality and Data Accuracy Requirements," AGARD-AR-184, Nov.1982, p.17.
9. Paquet, J.B., "Perturbations induites par les parois d'une soufflerie," Thèse Ing. Doc., Lille, June 1979, pp.69-71.